

## The electronic structure of a single-walled aluminosilicate nanotube

This article has been downloaded from IOPscience. Please scroll down to see the full text article.

2008 Nanotechnology 19 175702

(<http://iopscience.iop.org/0957-4484/19/17/175702>)

View [the table of contents for this issue](#), or go to the [journal homepage](#) for more

Download details:

IP Address: 134.147.88.26

The article was downloaded on 27/09/2011 at 02:35

Please note that [terms and conditions apply](#).

# The electronic structure of a single-walled aluminosilicate nanotube

Lijuan Li, Yueyuan Xia, Mingwen Zhao, Chen Song, Jiling Li and Xiangdong Liu

School of Physics and Microelectronics, Shandong University, Jinan, Shandong 250100, People's Republic of China

E-mail: [yyxia@sdu.edu.cn](mailto:yyxia@sdu.edu.cn)

Received 21 November 2007, in final form 15 February 2008

Published 25 March 2008

Online at [stacks.iop.org/Nano/19/175702](http://stacks.iop.org/Nano/19/175702)

## Abstract

The geometric structure and electronic structure of an imogolite nanotube have been studied using density functional theory (DFT). The calculation results indicate that the deformation of the material leads to structural electric charges on the tube wall. This hydrous aluminosilicate single-walled nanotube is a wide gap semiconductor with a direct band gap,  $E_g \sim 3.67$  eV at the  $\Gamma$  point, which may be promising for application in optoelectronic devices. In conjunction with the DFT calculations, molecular dynamics simulations based on empirical potentials are also performed to evaluate the mechanical properties of this material.

## 1. Introduction

Imogolite, a hydrous aluminosilicate with single-walled tubular structure, has attracted considerable attention in recent years [1–10]. This material has the composition of  $(\text{OH})_3\text{Al}_2\text{O}_3\text{SiOH}$ , and the structure of isolated imogolite can be described as a tube with the wall consisting of a curved gibbsite-like sheet with SiOH groups bound on the inner wall and Al–OH groups on the outer wall [11]. Based on earlier experimental studies [11, 12] and recent experiments using various characterization techniques [1], such as transmission electron microscopy (TEM), electron diffraction, x-ray diffraction, dynamic light scattering, and nitrogen adsorption, the unique structure of this material has basically been revealed. It is generally accepted that synthetic imogolite nanotubes are highly monodisperse in diameter, irrespective of different synthesis conditions [1]. The external diameter of the tube is  $\sim 2.2$  nm. The center-to-center separation of the tubes measured by TEM is 2.7–2.8 nm [6, 8] for synthetic imogolite, which may be larger than the real outer diameter of an isolated tube. The internal diameters of the imogolite nanotubes determined using adsorption analysis are in the range of 0.9–1.1 nm [6, 11], and the electron diffraction patterns gave a periodicity of 0.84–0.85 nm along the tube axis [1, 6, 11]. The synthetic imogolite nanotube was determined to have a circumference composed of 12 ( $N_u = 12$ ) gibbsite units, i.e. 24 Al atoms ( $n = 2N_u$ ) in the circumference [4, 6, 10]. Since the

imogolite tube has no chiral structure and is monodisperse in diameter, one would expect that the measurements of its physical properties should be more reproducible than those for the carbon nanotubes, whose electronic band structures are extremely sensitive to the helicity and diameter of individual nanotubes [13]. This monodispersity feature of imogolite single-walled nanotubes is essentially important for nanotechnology. Furthermore, the hydroxyl groups on the outer and inner walls of the nanotube make it very hydrophilic. The formation of a meso-structured well-crystallized synthetic imogolite with high meso-porosity has also been characterized [2]. These features of imogolite make this material particularly attractive for technical applications. For example, imogolite nanotubes have been considered as a potential multipurpose adsorbent, especially for methane storage [2], for use as a catalyst support [14, 15], a shape-selective catalyst [16], and molecular sieving [17]. The study of the water vapor adsorption isotherm indicated that synthetic imogolite showed a rapid increase of water adsorption at relative pressure over 90% and desorbed most of the absorbed water at relative pressure under 90% [2]. This property makes it suitable for repeated prevention of dew condensation. In the field of nanoelectronics, imogolite was proved to be an excellent electron emitter [18]. The functionalization of imogolite nanotubes to extend the application prospects and substitution of Ge for Si in imogolite to increase the diameter for use in artificial ion channel for biomolecule sensing devices were discussed in [6] and [1], respectively.

Although imogolite has shown great prospects, the research efforts given to this material are not as extensive as those for carbon nanotubes. In particular, studies on the application of imogolite for electronic and optoelectronic devices are rare. This may be caused by lack of available information on the electronic properties of this material. In this work we study the electronic structure of single-walled imogolite nanotubes by performing density functional theory (DFT) calculations to provide valuable information for predicting the electronic properties of this unique material. Since the mechanical property of a material is an important issue for its practical applications, we also studied the mechanical property of imogolite nanotubes by using molecular dynamics simulations (MDSs) based on the empirical force field method, instead of using MDSs based on DFT calculation.

## 2. Theoretical methods

A supercell of an imogolite single-walled nanotube was constructed based on the composition of  $(\text{OH})_3\text{Al}_2\text{O}_3\text{SiOH}$ , which had 12 gibbsite units ( $N_u = 12$ ) in the circumference and a repeat period of 0.85 nm in the axis direction. The supercell consisted of 336 atoms (24 silicon atoms, 48 aluminum atoms, 168 oxygen atoms and 96 hydrogen atoms). Previous MDSs using empirical potentials [4, 5] have shown that the energy per atom of the imogolite nanotubes has a minimum value at a certain  $N_u$  value. Konduri *et al* predicted that a minimum appeared at  $N_u = 12$  [4], whereas Tamura *et al* predicted a minimum at  $N_u = 16$  [5]. According to the recent experimental studies [1, 6], computer modeling to fit the experimental data of gases adsorption [10] and *NVT* MDS [4], it is more likely that the synthetic imogolite nanotubes have  $N_u = 12$ . Recently, an x-ray diffraction pattern (XRDP) simulation also indicated that  $N_u = 12$  gave a good agreement between the theoretical [19] and experimental results [1]. Therefore we adopted this value, rather than  $N_u = 16$ , to construct the supercell in this work. All the atomic coordinates in the supercell were relaxed using a conjugate gradient (CG) algorithm. The calculations were performed by using the computer code SIESTA [20–22], which is based on the standard Kohn–Sham self-consistent DFT. A flexible linear combination of numerical atomic orbitals (LCAO) was used to form basis sets for valence electrons, and nonlocal norm-conserving pseudopotential were adopted for the atomic cores. The pseudopotentials were constructed using the Trouiller–Martins scheme [23] to describe the interactions of valence electrons with the atomic cores. The nonlocal components of the pseudopotential were expressed in the fully separable form of Kleinman and Bylander [24]. The generalized gradient approximation (GGA) was used for the exchange–correlation potentials in terms of the Perdew, Burke and Ernzerhof scheme [25]. The atomic orbital set employed was a double- $\zeta$  plus polarization (DZP) function. The numerical integrals were performed and projected on a real space grid with an equivalent cutoff of  $120 R_y$  to calculate the self-consistent Hamiltonian matrix elements. A periodic boundary condition along the tube axis was employed with the lateral vacuum region large

enough (4 nm between the outer shells) to avoid the image interactions. Proper  $k$ -sampling for the Brillouin zone along the tube axis according to the Monkhorst–Pack method [26] was adopted to let the energy of the system converge to the order of 1 meV. The CG steps were continued to relax the supercell until the maximum force exerted on the atoms of the supercell was less than  $0.04 \text{ eV } \text{\AA}^{-1}$ . Once the system was fully relaxed and converged, the optimized configuration, the energy of the system and the details of the electronic structures of the system could be obtained.

To predict the mechanical properties of this material, we studied the behavior of stress versus strain for the single-walled imogolite tube by using MDSs based on the empirical force field method. Although the mechanical properties can also be studied, in principle, by use of DFT structural relaxation or a DFT-MDS method based on the energy changes of the supercell in response to the loading stress, the timescale needed for the dynamical structure equilibrium is long (at least several ps), and thus it is practically infeasible for such a big supercell as that under study to use the DFT-MDS method. Therefore we use the empirical force field method instead of the DFT method to obtain the Young's modulus. The interatomic potential set used in the simulations was selected from the Catlow library included in GULP computer code [27]. The electronic polarizability effects were taken into account by using the core–shell model [28] for the oxygen ions. The massless shell was linked to the core via harmonic interactions. The interactions between the cation cores ( $\text{Al}^{3+}$  and  $\text{Si}^{4+}$ ) and the  $\text{O}_{\text{shell}}$  and that of  $\text{O}_{\text{shell}}\text{--O}_{\text{shell}}$ , cation–OH, OH–OH and long-range O–H were described by Buckingham potentials. The intramolecular O–H interaction for the hydroxyl group was described by Morse potential. The three-body bond-bending interactions were considered for the O–Al–O octahedral group and the O–Si–O tetrahedral group to describe the covalent effects. These potential sets have been widely used to predict the structures and properties of aluminium silicate compounds [29] and the crystal lattice of clays [30]. For example, using these potentials with the optimized parameters, phyllosilicates with high interlayer charge, like muscovite and margarite, and 2:1 phyllosilicates with the minimal interlayer charge, like pyrophyllite  $[\text{Si}_4\text{Al}_2\text{O}_{10}(\text{OH})_2]$ , were simulated, and the simulation results reproduced the experimentally structural features of these materials very well, with bond length and bond angle deviation less than 2% from the experimental values [30]. The transferability of the potentials was also tested and found suitable for use in the simulation of a series of smectite and illites [30]. Because of the much lower computation requirement needed in comparison with DFT calculations, it is possible to use higher convergent criteria in the empirical modeling to increase the accuracy of the simulations. A larger supercell is proper for obtaining the Young's modulus by using the empirical MDS since it needs to exert constraints on the atoms of the supercell ends. The supercell used for the empirical modeling has a size twice as large as that used in the DFT calculations (two periods long in the axial direction, containing 672 atoms). A periodic boundary condition along the tube axis was adopted with

the lateral vacuum region to be 7 nm to avoid any effects of intertube interactions to simulate an isolated imogolite tube. The initially constructed structure of the imogolite nanotube was optimized by using the CG algorithm with the inverse Hessian updating scheme of Broyden–Fletcher–Goldfarb–Shanno [31]. The optimized structure was obtained when all the atoms in the supercell were fully relaxed to reach a state that the maximum gradient norm converged to  $0.001 \text{ eV } \text{\AA}^{-1}$  and the total energy of the system converged to  $5 \times 10^{-7} \text{ eV}$ . To obtain the Young's modulus of the single-walled imogolite nanotube at room temperature, the optimized structure was then subjected to MDS at  $T = 300 \text{ K}$  with an integration time step of 0.4 fs and a 2 ps equilibration state followed by a 50 ps data collection stage. The temperature was controlled by a Nosé–Hoover thermostat. The MDS indicated that the energy and temperature equilibrated well within 1–2 ps. This time interval for equilibration is in agreement with [4]. The average diameter of the imogolite tube was obtained from the MDS data. To obtain the stress–strain relationship, the end atoms of the tube were shifted along the axis by small steps and the whole tube was relaxed with MDSs at 300 K while keeping the tube ends constrained. From the relaxed structure and the energy change of the tube, the Young's modulus can be obtained. The MDSs were performed by using the GULP code [27].

### 3. Results and discussion

#### 3.1. The structure and deformation of the imogolite nanotube

The optimized configuration of an isolated single-walled imogolite nanotube obtained from the DFT calculations, viewed in the direction of the tube axis, is shown in figure 1(a). The detailed structures around an Al–O octahedron and a Si–O tetrahedron are shown in figures 1(b) and (c), respectively. The dashed trapezoid in this figure shows a gibbsite unit of the tube. The solid arrows and the dashed arrows with the label numbers point to the atom groups SiOH and AlOH, respectively, which are the most reactive groups and of importance for the electric structure of the tube. These atom groups are represented by SiOH( $x$ ) ( $x = 1, 2, 3, 12, 13, 14, 15$ ) and Al–OctaH( $x$ ) ( $x = 25, 27, 28, 29, 71, 72$ ), respectively, to distinguish them from other atoms or atom groups (see figure 4(c)). The outer diameter (measured between two opposite hydrogen atoms on the outer wall) of this imogolite tube is  $\sim 2.33 \text{ nm}$ , the internal diameter of the tube (measured between two opposite hydrogen atoms on the internal wall) is  $\sim 1.24 \text{ nm}$ , and the lattice period along the tube axis is  $\sim 0.87 \text{ nm}$ . These values are in good agreement with the experimental values of the external diameter [1, 6, 11], the internal diameter [6, 11], and the repeat unit length along the tube axis [1, 6, 11] for the imogolite nanotube. The average Si–O, Al–O and O–H bond lengths are 0.169, 0.194 and 0.097 nm, respectively, which agree with the corresponding values reported in [5], i.e. 0.162, 0.196, and 0.098 nm for the Si–O, Al–O and O–H bonds respectively. In fact, the values of the bond lengths reported in [5] were obtained by adjusting the parameters of the empirical potentials in their MDSs to reproduce the experimental structures of

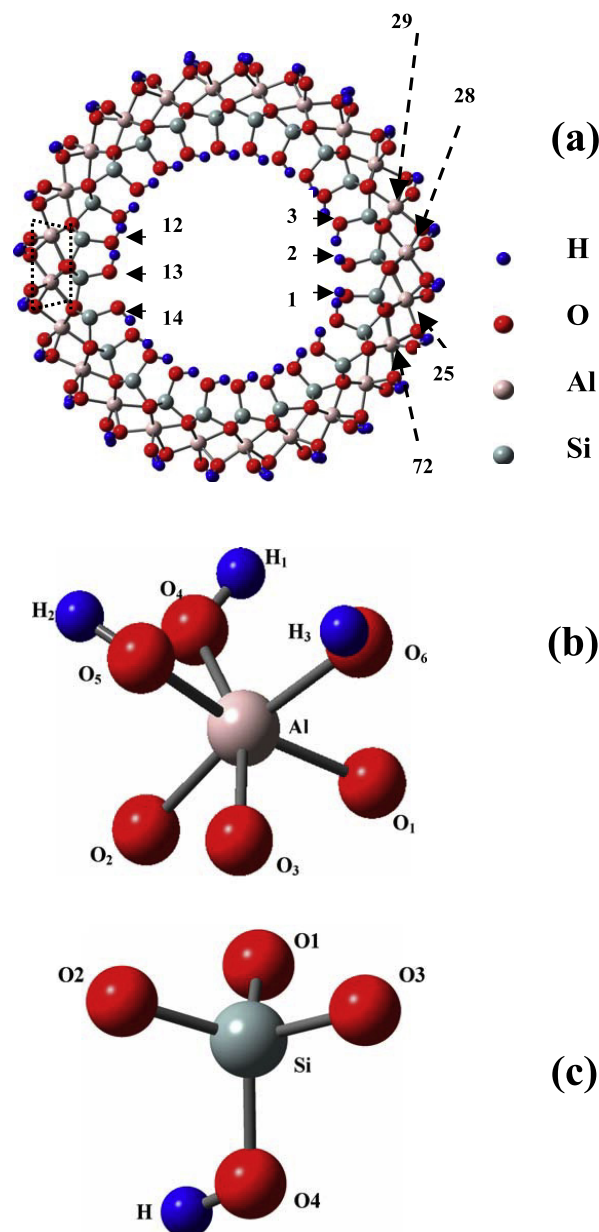


**Figure 1.** The optimized configuration of a single-walled imogolite nanotube. (a) The top view along the tube axis: the dashed trapezoid shows a gibbsite unit, and the solid (dashed) arrows with label numbers point to the SiOH (AlOH) atom groups, which are most active (cf the text and figure 4(c)), (b) the Al–O octahedron structure in the gibbsite-like curved sheet, (c) the Si–OH tetrahedron structure on the inner wall.

gibbsite, silicate and the hydroxyl group, OH. This indicates that the bond lengths of the optimized configuration obtained from the present DFT calculation reproduce the experimental bond lengths very well. Table 1 lists the geometric structure parameters of the imogolite tube compared with experimental values. From table 1, it is evident that the bond lengths of the Al–O octahedra, the Si–O tetrahedra and the OH groups in the imogolite tube are close to the corresponding values of bulk silicate materials, which even have various cation substitutional chemical compositions. But the curvature and the strain induced by the tubular structure of the imogolite

**Table 1.** Geometrical parameters of the imogolite nanotube: comparison between the theoretical results and experimental results.

Geometrical parameters of imogolite	Calculation	Experiments
Outer diameter (nm)	2.33	2.2 <sup>a</sup> , 2.4 <sup>b</sup>
Inner diameter (nm)	1.24	0.9 <sup>b</sup> , 1.12 <sup>c</sup>
Repeat period in axial direction (nm)	0.87	0.85 <sup>a</sup> , 0.84 <sup>b</sup>
Al–O average bond length (nm)	0.194	0.191 <sup>d</sup> , 0.194 <sup>e</sup> , 0.192 <sup>f</sup>
Si–O average bond length (nm)	0.169	0.1643 <sup>e</sup> , 0.1636 <sup>f</sup>
O–H bond length (nm)	0.097	0.0947 <sup>e</sup> , 0.0941 <sup>g</sup>
Bond Angle (deg)		
Tetrahedral	O <sub>1</sub> –Si–O <sub>2</sub> 106.8, O <sub>1</sub> –Si–O <sub>3</sub> 109.2 O <sub>2</sub> –Si–O <sub>3</sub> 113.3, O <sub>1</sub> –Si–O <sub>4</sub> (H) 113.5 O <sub>2</sub> –Si–O <sub>4</sub> (H) 109.0, O <sub>3</sub> –Si–O <sub>4</sub> (H) 105.1 Mean O–Si–O 109.5	109.5 <sup>f</sup> , 110.4 <sup>g</sup>
Octahedral	O <sub>1</sub> –Al–O <sub>2</sub> 100.0, O <sub>1</sub> –Al–O <sub>3</sub> 87.0 O <sub>2</sub> –Al–O <sub>3</sub> 93.7, O <sub>2</sub> –Al–O <sub>5</sub> 93.7 O <sub>1</sub> –Al–O <sub>5</sub> (H <sub>2</sub> ) 160.3, O <sub>1</sub> –Al–O <sub>6</sub> (H <sub>3</sub> ) 78.4 O <sub>2</sub> –Al–O <sub>4</sub> (H <sub>1</sub> ) 77.7, O <sub>2</sub> –Al–O <sub>5</sub> (H <sub>2</sub> ) 95.0 O <sub>2</sub> –Al–O <sub>6</sub> (H <sub>3</sub> ) 167.1, O <sub>3</sub> –Al–O <sub>4</sub> (H <sub>1</sub> ) 170.9 O <sub>3</sub> –Al–O <sub>5</sub> (H <sub>2</sub> ) 79.3, O <sub>3</sub> –Al–O <sub>6</sub> (H <sub>3</sub> ) 99.0 O <sub>4</sub> (H <sub>1</sub> )–Al–O <sub>5</sub> (H <sub>2</sub> ) 104.0, O <sub>4</sub> (H <sub>1</sub> )–Al–O <sub>6</sub> (H <sub>3</sub> ) 89.5 O <sub>5</sub> (H <sub>2</sub> )–Al–O <sub>6</sub> (H <sub>3</sub> ) 89.7	

<sup>a</sup> Reference [1].<sup>b</sup> Reference [6].<sup>c</sup> Reference [11] deduced from the adsorption data of Wada and Henmi.<sup>d</sup> Reference [36] determined based on the diffractometer data of gibbsite.<sup>e</sup> Reference [37] experimental data of muscovite.<sup>f</sup> Reference [38] experimental data of Panasqueira muscovite.<sup>g</sup> Reference [39] experimental data of margarita.

make the Al–O octahedron (figure 1(b)) and the Si–O tetrahedron (figure 1(c)) deviate from an ortho-octahedral structure and an ortho-tetrahedral structure, respectively. For an ortho-octahedron the ideal bond angle should be 90° and that for an ideal ortho-tetrahedron should be 109.5°. However, the Al–O octahedron shown in figure 1(b) has bond angles substantially deviating from 90°. The O–Al–O bond angles of the octahedron vary from 77.7° to 170.9°, and the O–Si–O bond angles of the tetrahedron vary from 105.1° to 113.5°. The Al–O and Si–O bond lengths of both the Al–O octahedra and the Si–O tetrahedra are not very different from their average values, with the bond lengths being Al–O = 0.194 ± 0.006 nm and Si–O = 0.169 ± 0.004 nm. Thus the deformation of the tube is mainly characterized by the bond angle changes. It is obvious that the Al–O octahedra are severely deformed due to the curling of the gibbsite-like sheet into a tube, whereas the inner tetrahedral O<sub>3</sub>SiOH groups are less deformed.

A detailed theoretical study [32] indicated that the curvature of the imogolite tubes in their circumferences caused the substantial structural changes of the bond angles of the Al octahedra that form the outer part of the imogolite tubes. Our DFT calculations support this theoretical analysis.

Besides the deformation of the Al–O octahedra and Si–O tetrahedra of the tube, the curling of the gibbsite sheet and the associated Si–OH group also makes the global structure of

the tube deformed. As a material with partial ionic bonds, the deformation of the imogolite nanotubes will certainly give rise to electric charge redistribution, and thus cause the change of the surface electric charges. The surface charges induced by the structure changes (named as structural charges) have been predicted [32]. In this context, we analyze the deformation and relevant surface charge of this material structure in a detailed way. To show the local curvature of the circumference of the tube, a patch cut from the cylindrical tube wall is presented in figure 2(a). From the inner to outer layers, the OH, Si, O, Al and OH groups are located on different circles with the diameters gradually increasing. The distance between two outer wall OH groups, which are the nearest neighbors on a circle of the circumference, is about 5.75 Å, while that between two nearest O atoms on a circle, which are shared by Al atoms and Si atoms, is about 4.67 Å (figure 2(a)). Figure 2(b) is a top view of the patch to show the distance between the two nearest Al atoms on a circle and that between two nearest Si atoms on a circle of the inner layer. The direction of the tube axis, *z*, is shown in the right side of figure 2(b) by an arrow surrounded by a circle representing a tube along the *z*-axis. It is obvious that the distances between the OH groups on the outer wall are lengthened, whereas those between the O groups shared by Al and Si atoms in the inner layer are shortened. The distances between the Al atoms and those between the Si atoms



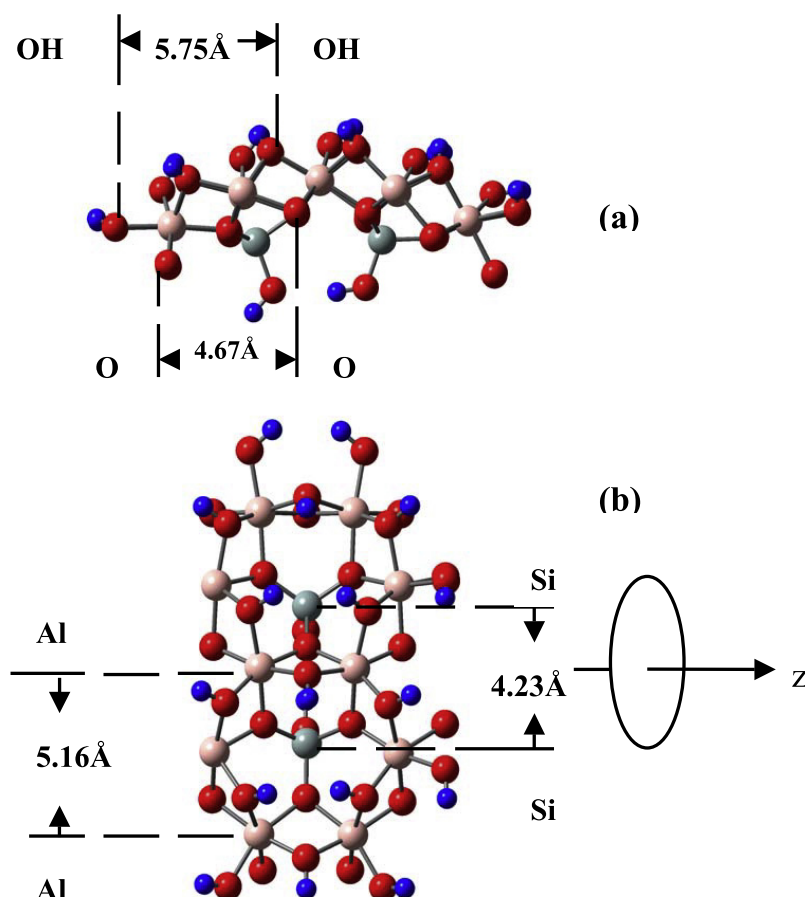


**Figure 2.** The curvature of the imogolite nanotube leads to lengthening of the distance between the outer layer atoms and shortening of that between the inner layer atoms.

are correspondingly changed. Let us see what happens to the electric charges in response to these deformations in the imogolite nanotube.

### 3.2. The electric dipole and surface charges of the imogolite nanotube

Our calculation results indicate that the optimized configuration of the imogolite tube, shown in figure 1(a), has an electric dipole of 18.93 debye in the direction of the  $x$ -axis ( $\mathbf{P} = 18.93\mathbf{i} + 1.08\mathbf{j} - 0.0088\mathbf{k}$ ;  $P_y$  and  $P_z$  are much less than  $P_x$ ), which is chosen along the tube diameter in the horizontal direction of figure 1(a), although the imogolite is electrically neutral. The existence of this global electric dipole makes the hydrogen atoms of the OH groups, especially those hung on the inner wall, orient in an ordered manner, since the hydrogen atoms of the OH groups are bearing electric charges. As shown in figure 1(a), the diameter in the horizontal direction (the  $x$ -axis) divides the geometric cross section of the tube into two parts. The internal hydrogen atom rings are oriented clockwise in the upper part and anticlockwise in the lower part. To give the physical reason for this, we calculated the local electrostatic charge distribution based on the Mulliken population analysis. In figure 3(a), the thick dashed line shows the  $x$ -axis,

along which there is an electric dipole of 18.93 debye. On the left side of this figure, there are two regions surrounded by the dashed lines and labeled A and B, respectively. Correspondingly, on the right side there are two regions labeled C and D, respectively. Both regions A and B on the left side have local negative charges ( $-0.196e$  and  $-0.046e$ , respectively), whereas the regions C and D on the right side have opposite signs of charges ( $+0.03e$  and  $-0.194e$ , respectively). The electric lines of force around the global dipole moment  $P_x$  are schematically shown in figure 3(b). The DFT calculation indicates that each OH on the inner wall has an average local dipole moment  $\sim 0.64$  debye. The field produced by the global dipole  $P_x$  will make the OH dipoles orientate along the lines of force to form a special pattern of clockwise and anticlockwise hydrogen rings on the inner wall, as observed in figures 1(a) and 3(a). Another interesting issue is the surface electric charges, which are essential to determine the adsorption properties and the reactivity of this material, for instance the capacity for cation adsorption and stabilization of metallic particles [33]. The Mulliken population analysis for the optimized structure of the imogolite shown in figure 1(a) indicates that the electrons transfer from Al atoms and Si atoms to the O atoms in the middle layers, which are shared by the Al and Si atoms, such as the oxygen atoms labeled by  $O_1$ ,  $O_2$  and

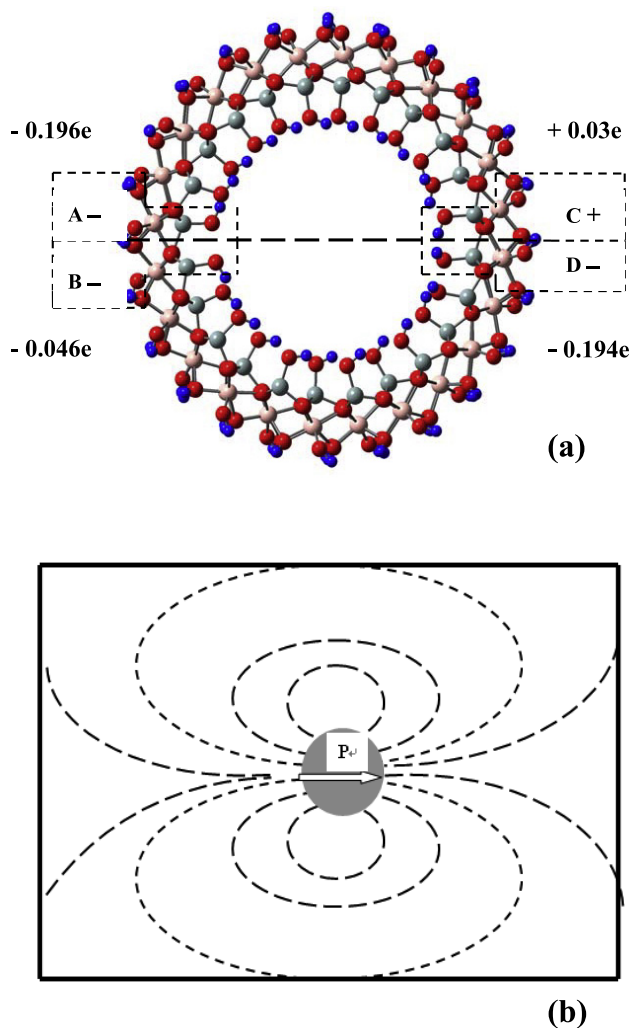


**Figure 3.** Local electric charge and the electric dipole induced by the deformation of the imogolite nanotube make the inner hydrogen rings orientate clockwise and anticlockwise.

O<sub>3</sub> shown in figures 1(b) and (c). As a result, weak positive charges are induced on the outer surface of the tube. The positive charges are contributed from all the Al–OH groups on the outer surface. This is in agreement with the result obtained by the structural analysis and the bond valence calculations for the imogolite tube with  $N_{\mu} = 12$  [32]. Due to lack of accurate structural information about imogolite tubes, in [32] Gustafsson used a postulation, i.e. the mean Al–O bond length is slightly longer for the Al–O–Al bonds bridging the tetrahedral Si, as compared with the outer Al–OH–Al bonds. Our DFT results indicate this is true: the mean Al–O bond length between the Al atoms and the O atoms, which are shared by Al and Si, is really a bit longer than that of Al–O for the outer wall Al–OH–Al bonds. Therefore, the present detailed structure calculation for the imogolite tube may provide useful information for further studies of the surface electric charges on imogolites. There are also differences between the structural charges obtained from the present DFT calculation and those predicted in [32] according to the assumed structure of the imogolite tube. Gustafsson predicted that the inner wall of

the tube was negatively charged [32], whereas our result indicates that the electric charges on the inner wall are distributed more complicatedly. The present result shows that the electric charges on the inner wall are site dependent. Some of the OH hydroxyls on the inner wall are positively charged but others are negatively charged. This is caused by the structure fluctuations of the Al–O octahedra and Si–O tetrahedra of the material. Although each Al–O octahedron and Si–O tetrahedron is similar to their corresponding coordinate units in the imogolite, as the representative configurations shown in figures 1(b) and (c), respectively, upon detailed analysis of the structure for each one of them we found that small diversities of both the bond angles and the bond lengths occur. Even the global structure of the imogolite deviates slightly from an ideal cylindrical configuration. The nonuniformity of the practical structure of the imogolite may lead to the site-dependent charge distribution on the inner wall and the electric dipole in the  $x$ -axis direction. From the Mulliken charge analysis, we know that each OH on the outer wall of the imogolite has an average negative charge  $\sim -0.034\,19e$ , and each Al cation in the Al–(OH)<sub>3</sub> on the outer wall has an average positive charge of  $+0.205e$ , of which half contributes to the surface charge and other half contributes to the bonds connecting the inner three O anions. Thus we can count all the charges on the outer surface of the supercell, that is about  $+2.46e$ . The surface area of the supercell is about  $6.39 \times 10^{-18}\,\text{m}^2$ . We estimate the surface charge density on the outer wall to be  $\sim 62\,\text{mC m}^{-2}$ , in comparison with the value of  $20\text{--}40\,\text{mC m}^{-2}$  estimated in [32]. Experimental studies have proved that imogolite can adsorb both cations and anions. Besides the specific adsorptions, the experimental evidence indicated that some cations are adsorbed via electrostatic interactions [34] on the inner wall of the imogolite tube. The fact that small cations are adsorbed in the hollow tubes of imogolite was further supported by an experimental fluorescence study [35]. The existence of negatively charged sites on the inner wall of the imogolite predicted by the present work is consistent with this experimental evidence.

### 3.3. Energy bands and electron density of states of imogolite

Studies of the electronic structure of imogolite are essentially important for exploring potential applications of this material in electronic and optoelectronic devices. The present DFT calculations have provided the energy bands and associated electron density of states of this material. Figure 4 shows the energy band structure and the electron density of states near the Fermi level for a single-walled imogolite nanotube. The Fermi level of this material structure is set at  $E = 0$ , and is indicated by the dashed lines in the middle of the gap. The energy bands depicted in figure 4(a) clearly indicate a direct band gap with energy gap of  $E_g \sim 3.67\,\text{eV}$  at the  $\Gamma$  point. The imogolite nanotube is thus predicted to be a wide band gap semiconductor with a direct gap. This feature is particularly attractive for application in optoelectronic devices working in the ultraviolet region since materials with direct gaps usually have higher optical emission and absorption intensities than indirect gap materials. Figure 4(b) shows the electron density of states (DOS) near the Fermi level. The energy position

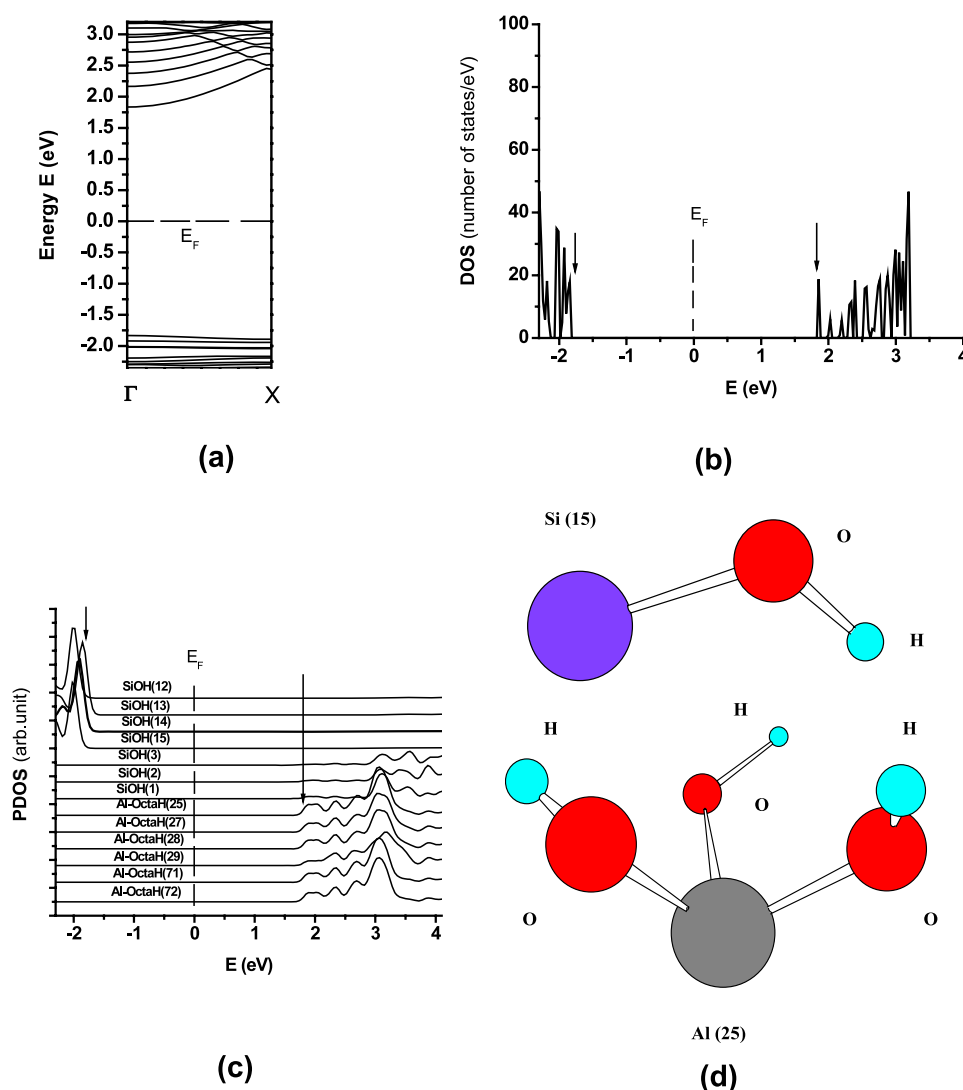


**Figure 4.** The energy bands of the single-walled imogolite nanotube and the electron density of states: (a) the energy bands near the Fermi level, showing the direct and wide energy gap, (b) the total electron density of states, (c) the projected electron density of states near the Fermi level, showing different atom groups contributing to the states near the top of the valence bands and near the bottom of the conduction bands, and (d) two atomic groups relevant to the labels in (c).

(This figure is in colour only in the electronic version)

of the top of the valence band and that of the bottom of the conduction band are indicated by the arrows in this figure. It is evident that the energy gap shown in the DOS (figure 4(b)) just corresponds to the energy band gap shown in figure 4(a). Since the electron states close to the top of the valence band and at or close to the bottom of the conduction band are taking the most important role for the chemical and electronic or optoelectronic properties of the material, we focus our attention on these states. To find out which atoms or atomic groups contribute to the electron states near the top of the valence band and near the bottom of the conduction band, we calculated the projected density of states (PDOS) of the imogolite by projecting the total density of states onto the basis orbitals for the selected atomic groups, and plotted them in figure 4(c). The contribution to the PDOS from different atomic groups is labeled in this figure. The numbers in the brackets are used to distinguish the Si–OH and Al–OH

atomic groups (marked by the arrows with the label numbers in figure 1(a)) from other atoms and atom groups in the supercell. To illustrate the meaning of these labels, in figure 4(d) we give the configurations of a Si–OH atomic group and an Al–OH atomic group, which represent the groups labeled by SiOH(15) and Al-OctaH(25), respectively, in figure 4(c). The other labels in figure 4(c) represent similar structures of the atomic groups. From the PDOS, it is obvious that the states near the top of the valence band are mainly contributed from some of the SiOH groups on the left side of the inner wall of the imogolite tube, while the states near the bottom of the conduction band are mainly due to the Al–OH groups on the right side of the outer wall of the imogolite tube (see the label numbers on figure 1(a)) with a small contribution from the SiOH groups in the inner wall. This feature may be explained by the energy shifts caused by the electric field [40]. The dipole  $\mathbf{P}$  has the negative pole on the left side and the positive



pole on the right side. From figure 3(b), one finds that the lines of force are denser near the pole area, thus having higher electric field there. The electric field causes the energies of electrons shifting upwards on the left side and downwards on the right side. Therefore, the energies of the electron states of the SiOH groups on the left side may be shifted upwards to form the bands on the top of valence bands, and those of the electron states of the Al–OH groups on the right side may be shifted downwards to form the bands on the bottom of the conduction bands. The shifts are different due to the electric field distribution. This feature also indicates that the most reactive sites are located on the outer and inner surfaces of the imogolite. Considering this feature and the surface electric charges of the imogolite discussed above, it seems that functionalization of the imogolite tube to extend its application prospects may be easily achieved by simply adsorbing or doping with properly selected atoms, molecules or radicals on the outer wall or the inner wall. Functionalization of the single-walled imogolite nanotube is a subject worthy to be further studied.

The mechanical property of imogolite nanotubes is another subject which is important for applications of this material. From our MDS data obtained from the GULP code using the empirical force fields, we analyzed the energy change of the supercell when it was lengthened along the tube axial by a small strain  $\sim 0.005$ . When the MDS was performed for 52 ps, we found that the average diameter of the imogolite decreased to respond to the axial lengthening. From the change of the diameter and the axial strain, we obtained the Poisson's ratio of the imogolite nanotube,  $\gamma \sim 0.39$ . Unlike the macroscopic continuum materials, where the Young's modulus can be accurately determined by using the simple relationship between the tensile stress and the corresponding tensile strain, it is difficult to determine the Young's modulus accurately for a nanotube since the wall thickness of the nanotube is not exactly known. One cannot just determine the wall thickness according to the positions of the nuclei of the atoms because the valence electrons may extend to a range comparable to the radius of the nanotubes. This problem has puzzled those who have been studying the mechanical properties of carbon nanotubes since carbon nanotubes were discovered. In the present work, we use the experimentally measured center-to-center spacing (2.7 nm) as the effective outer diameter of the imogolite tube and the experimentally determined internal diameter (0.9 nm) [6] as the effective internal diameter to obtain the wall thickness of the single-walled imogolite nanotube. This estimation for the thickness of the wall is reasonable from the point of view of the lateral distribution of the valence electrons. The integral charge distribution from the DFT calculations indicates that most of the valence electrons are distributed within 2 Å from the positions of the nuclei. The outer radius of the theoretical value plus 2 Å just forms an effective outer diameter of  $\sim 2.7$  nm, which is very close to the experimentally observed center-to-center spacing. Similarly, we can justify the use of the experimentally observed inner diameter for estimating the wall thickness. Using this thickness and the relationship between the stress and strain, we obtain the Young's modulus of the imogolite tube,  $Y \sim 182.6$  GPa.

## 4. Conclusions

In summary, the atomistic structure and the electronic structure of a single-walled imogolite tube have been studied by using DFT calculations. The detailed structural parameters are obtained, which are in agreement with the experimental values. The deformation of the material and associated structural charges, i.e., the electric dipole and the surface electric charges, are studied. The surface electric charges obtained from this work are consistent with the good adsorption capacity of the material found experimentally for both cations and anions. The energy bands of the imogolite nanotube are reported for the first time. They indicate that a single-walled imogolite nanotube is a wide band gap semiconductor with a direct gap. Therefore it may be a promising material for application in optoelectronic devices working in the ultraviolet wavelength region. The PDOS result indicates that the electronic states near the top of the valence bands and those near the bottom of the conduction bands are mainly contributed from the SiOH groups in the inner wall and the Al–OH groups in the outer wall, respectively. The primary mechanical property is estimated by using MDSs based on the empirical force fields, and the Young's modulus and the Poisson ratio of this material are given.

## Acknowledgments

We are grateful to Dr Professor J Gale for providing us with the GULP 3.0 code. This work is supported by the National Natural Science Foundation of China under grant Nos 10675075 and 50402017, and supported by the National Basic Research Program of China under grant No. 2005CB623602.

## References

- [1] Mukherjee S, Bartlow V M and Nair S 2005 *Chem. Mater.* **17** 4900
- [2] Ohashi F, Tomura S, Akaku K, Hayashi S and Wada S-I 2004 *J. Mater. Sci.* **39** 1799
- [3] Ohrai Y, Gozu T, Yoshida S, Takeuchi O, Iijima S and Shigekawa H 2005 *Japan. J. Appl. Phys.* **44** 5397
- [4] Konduri S, Mukherjee S and Nair S 2006 *Phys. Rev. B* **74** 033401
- [5] Tamura K and Kawamura K 2002 *J. Phys. Chem. B* **106** 271
- [6] Bursill L A, Peng J L and Bourgeois L N 2000 *Phil. Mag. A* **80** 105
- [7] Lee Y, Kim B, Yi W, Takahara A and Sohn D 2006 *Bull. Korean Chem. Soc.* **27** 1815
- [8] Koenderink G H, Kluijtmans S G J M and Philipse A P 1999 *J. Colloid Interface Sci.* **216** 429
- [9] Ackerman W C, Smith D M, Huling J C, Kim Y-W, Bailey J K and Brinker C J 1993 *Langmuir* **9** 1051
- [10] Pohl P I, Faulon J-L and Smith D M 1996 *Langmuir* **12** 4463
- [11] Cradwick P D G, Farmer V C, Russell J D, Masson C R, Wada K and Yoshinaga N 1972 *Nat. Phys. Sci.* **240** 187
- [12] Wada K, Yoshinaga N, Yotsumoto H, Ibe K and Aida S 1970 *Clay Min.* **8** 487
- [13] Mintmire J W, Dunlap B I and White C T 1992 *Phys. Rev. Lett.* **68** 631

- [14] Imamura S, Kokubu T, Yamashita T, Okamoto Y, Kajiwaru K and Kanai H 1996 *J. Catal.* **160** 137
- [15] Marzan L L and Philipse A P 1994 *Colloids Surf. A* **90** 95
- [16] Imamura S, Hayashi Y, Kajiwaru K, Hoshino H and Kaito C 1993 *Ind. Eng. Chem. Res.* **32** 600
- [17] Sehgal R, Huling J C and Brinker C J 1995 *Proc. 3rd Int. Conf. on Inorganic Membranes (Worcester, MA)* ed Y Ma p 85
- [18] Oh J, Lee Y, Sohn D, Chang S, Roh S and Yi W 2004 *Technical Digest of the 17th Int. Conf. (Cambridge, MA, July 2004)* ed A I Akinwande, L Chen, I Kymissis and C Hong pp 202–3 (IEEE Cat. No. 04TH8737)
- [19] Alvarez-Ramirez F 2007 *Phys. Rev. B* **76** 125421
- [20] Ordejón P, Artacho E and Soler J M 1996 *Phys. Rev. B* **53** R10441
- [21] Sánchez-Portal D, Ordejón P, Artacho E and Soler J M 1997 *Int. J. Quantum Chem.* **65** 453
- [22] Soler J M, Artacho E, Gale J, García A, Junquera J, Ordejón P and Sánchez-Portal D 2002 *J. Phys.: Condens. Matter* **14** 2745
- [23] Troullier N and Martins J L 1991 *Phys. Rev. B* **43** 1993
- [24] Kleinman L and Bylander D M 1982 *Phys. Rev. Lett.* **48** 1425
- [25] Perdew J P, Burke K and Ernzerhof M 1996 *Phys. Rev. Lett.* **77** 3865
- [26] Monkhorst H J and Pack J D 1976 *Phys. Rev. B* **13** 5188
- [27] Gale J D 1997 *J. Chem. Soc. Faraday Trans.* **93** 629
- [28] Dick B G and Overhauser A W 1958 *Phys. Rev.* **112** 90
- [29] Schröder K P, Sauer J, Leslie M, Catlow C R A and Thomas J M 1992 *Chem. Phys. Lett.* **188** 320
- [30] Sainz-Diaz C I, Hernández-laguna A and Dove M T 2001 *Phys. Chem. Minerals* **28** 130
- [31] Shanno D F 1970 *Math. Comput.* **24** 647
- [32] Gustafsson J P 2001 *Clays Clay Minerals* **49** 73
- [33] Yamada H, Michalik J, Sadlo J, Perlinska J, Takenouchi S, Shimomura S and Uchida Y 2001 *Appl. Clay Sci.* **19** 173
- [34] Denaix L, Lamy I and Bottero J Y 1999 *Colloids Surf. A* **158** 315
- [35] Harsh J B, Traina S J, Boyle J and Yang Y 1992 *Clays Clay Minerals* **40** 700
- [36] Saalfeld H and Wedde M 1974 *Z. Kristallogr. Bd.* **139** 129
- [37] Catti M, Ferraris G, Hull S and Pavese A 1994 *Eur. J. Mineral.* **6** 171
- [38] Guggenheim S, Chang Y-H and Koster van Groos A F 1987 *Am. Mineral.* **72** 537
- [39] Kassner D, Baur W H, Joswig W, Eichhorn K, Wendschuh-Josties M and Kupcik V 1993 *Acta Crystallogr. B* **49** 646
- [40] Son Y-W, Cohen M L and Louie S G 2006 *Nature* **444** 347